

Received 4 April 2023, accepted 14 April 2023, date of publication 18 April 2023, date of current version 28 April 2023.

Digital Object Identifier 10.1109/ACCESS.2023.3268029

## RESEARCH ARTICLE

# Design of a Low-Profile Dual Linearly Polarized Antenna Array for mm-Wave 5G

MARCO SIMONE<sup>1</sup>, SANTI CONCETTO PAVONE<sup>1,2,3</sup>, (Senior Member, IEEE),  
MATTEO BRUNO LODI<sup>1,3</sup>, (Member, IEEE), NICOLA CURRELI<sup>4</sup>, (Member, IEEE), GIACOMO MUNTONI<sup>1,3</sup>,  
ALESSANDRO FANTI<sup>1,3</sup>, (Senior Member, IEEE), GINO SORBELLO<sup>2,3</sup>, (Member, IEEE),  
AND GIUSEPPE MAZZARELLA<sup>1,3</sup>, (Senior Member, IEEE)

<sup>1</sup>Department of Electrical and Computer Engineering, University of Cagliari, 09123 Cagliari, Italy

<sup>2</sup>Department of Electrical, Electronics, and Computer Engineering (DIEEL), University of Catania, 95125 Catania, Italy

<sup>3</sup>Consorzio Interuniversitario per le Telecomunicazioni (CNIT), 43124 Parma, Italy

<sup>4</sup>Functional Nanosystems, Istituto Italiano di Tecnologia (IIT), 16163 Genoa, Italy

Corresponding author: Alessandro Fanti (alessandro.fanti@unica.it)


This work was supported in part by Ministero dello Sviluppo Economico “Monifive” under Project F94I20000100001. The work of Santi Concetto Pavone was supported by the Programma Operativo Nazionale (PON) Research and Innovation Attraction and Mobility of Researchers (AIM) Project, Action I.2, through the Fondo Sociale Europeo (FSE) European Union Program.

**ABSTRACT** This work proposes a dual linearly polarized antenna array for 5G mm-wave band, which is designed to be compatible with planar printed circuit board technology. The proposed antenna is engineered with a focus on simplifying the antenna geometry and eliminating any critical issues that may arise in antenna manufacturing. The proposed antenna has been evaluated, finding a 7% impedance bandwidth centered around 27.28 GHz. Additionally, the beam steering capability of the antenna is found to cover a  $\pm 30\%$  angular width for both linear polarizations. These findings highlight the potential of the proposed antenna for use in 5G mm-wave band applications, where compatibility with planar printed circuit board technology and simplified antenna geometry are essential design requirements.

**INDEX TERMS** 5G, antennas, array, beam steering, cross-dipole, dual linear polarization.

## I. INTRODUCTION

Wireless communication systems based on fifth-generation (5G) millimeter wave (mm-Wave) are considered to be modern and innovative technologies that are required for industrial, healthcare and Internet of Thing (IoT) applications [1], [2], [3]. Research and development on mm-Wave 5G systems are a clear industrial and social necessity, driven by the challenges of antenna and array design [4], [5]. The high-bandwidth requirement to meet the increasing demand for information transfer has needed the efficient exploitation of previously unavailable portions of electromagnetic (EM) spectrum [3]. The 24 – 28.5 GHz band is the candidate in mm-Wave 5G spectrum suggested by the U.S. Federal Communications Commission (FCC) and the European Union (EU) [4]. Technological issues are few at sub-6 GHz

The associate editor coordinating the review of this manuscript and approving it for publication was Kai-Da Xu .

bands, [4], [5], and lumped elements or artificial magnetic conductors can be used to enhance antenna performances [6]. At mm-Wave frequencies, to enable efficient links, antennas must be low-profile, compact, and low-cost, while also supporting high-gain and isolated dual polarization [5].

One of the key challenges in mm-Wave 5G antenna technology is the development of systems that are compatible with inexpensive front-ends capable of supporting phase-only beamforming [5]. Several configurations have been proposed and investigated [5], [7], [8], [9], [10], [11], [12], [13], including an eight-element phased array configuration for 3D-coverage beam scanning. However, some of these designs present the drawback of being cumbersome and too large to be integrated with front-end modules and integrated circuits (ICs) [4], [7]. To address this issues, it has been explored the use of compact and low-cost devices such as printed circuit boards (PCBs). For example, Haraz et al. [8], designed a dense dielectric patch antenna that was used in a

TABLE 1. mm-wave 5G antennas and arrays.

	[5]	[8]	[9]	[10]	[11]	[12]	[13]	This work
Basic Element	Lens	DDR	Patch	Dipoles	Patch	Patch	Dipoles	Dipole
Feeding Strategy	LWA	Microstrip	Aperture coupling	Coaxial	Microstrip	Coupling	Coaxial	CPW
Number of Elements	4×4	1x4	8x8	4×4	4×4	4×4	4x6	4×4
Bandwidth (%)	22.5	6.8	10.7	4.6	5	25	3.2	7
Maximum Gain (dBi)	27.5	16.3	21	16	6	19	8	16.25
Radiation Efficiency (%)	-	-	-	96	51	-	82	93
Scanning Angle (°)	±20	-	-	±20	-	±25	-	±30
Profile Height (mm)	12	2	2.7	4.64	5	<1	0.6	1.605
Size (mm <sup>2</sup> )	130x134	20x20	10.5x15.8	2500	34x31	-	2500	29.5x29.5
Monolithic	NO	NO	NO	NO	YES	YES	YES	YES
Manufacturing Technology	PCB	PCB	AiP	SIW	PCB	PCB	PCB	PCB
Optimization	YES	NO	NO	NO	YES	YES	YES	NO

DDR = Dielectric Dense Resonator, PCB = Printed Circuit Board, LWA = Leaky Wave Antenna, CPW = Coplanar Waveguide, AiP = Antenna-in-Package, SIW = Substrate Integrated Waveguide

1 × 4 phased array which demonstrated a gain of 16.3 dBi and an impedance bandwidth (BW) of about 6.8%. More recently, high-complexity layouts for antenna-in-package assembly have been proposed, such as the 64-element dual-polarized array described in [9].

The requirement for high-gain 5G antennas arises from the significant signal attenuation caused by oxygen molecules at mm-Wave [10]. To address this issue, a 4 × 4 array consisting of substrate integrated waveguide (SIW) cavity antennas was designed, fabricated, and tested. The array demonstrated a 4.6% BW, a maximum gain of approximately 16 dBi, and a scanning angle of ±20° [10]. Despite its good performances, the SIW array has a relatively high profile of around 4 mm, and losses cannot be neglected [10].

At higher microwave frequencies, it is often desirable to use circularly polarized antennas for both far-field [10], [11], [14] and near-field [15] applications, to minimize multipath interference and reduce the polarization mismatch. However, linearly polarized reconfigurable metasurface antennas have also been designed for microwaves [16]. In [11], an optimized polarization-reconfigurable microstrip-fed 4 × 4 patch antenna array was proposed. The PIN diodes biasing allowed to achieve the switching between left- and right-hand circular polarizations, while resulting in a structure of 5 mm height, with a maximum gain of 6 dBi and 5% BW [11].

Mao et al. [12] developed a broadband (25% BW), low-profile (<1 mm) microstrip 4 × 4 array for massive multi-input multi-output (MIMO) applications, using PCB technology. The array demonstrated a maximum gain of about 19 dBi, realizing a ±25° scanning angle. Recently, an optimized leaky wave antenna (LWA)-fed lens phased array with dual polarization was designed and fabricated, achieving a gain of 27 dBi, and ±20° scanning capability, but with a profile height of about 12 mm [5].

Although great efforts have been dedicated to compact 5G architectures in recent years, few arrays with the required performance have been reported in literature. Table 1 summarizes the currently available mm-Wave 5G arrays. Based on this analysis, it is evident that there is room for designing a 5G mm-Wave antenna which can outperform

the aforementioned designs while also ensuring technological feasibility and ease of manufacturing.

To advance the development of 5G mm-Wave devices and encourage their widespread adoption, a design approach guided by a technology-oriented perspective is essential, irrespective of the manufacturing technology employed. In this work we propose a low-complexity, low-profile, compact, and cost-effective 4 × 4 antenna array, suitable for manufacturing using PCB technology. The choice of PCB technology impacts the antenna design process, by imposing constraints on the antenna geometry, such as the vias diameter, their positioning with respect to the dipoles, and the conductive track size. However, this technology is low-cost and allows an easy integration, making it suitable for the arrangement of multilayer devices, even at mm-wave frequency range [17]. The simplicity of its geometry and ease of manufacturing ensure a good agreement between the simulated and measured results for the antenna [17], [18]. These advantages make it one of the most convenient technologies for antenna applications, up to high frequencies beyond 100 GHz [19]. To simplify the stack-up complexity and reduce costs, the antenna layout has been designed to integrate the feeding network in the same PCB laminate on which the antennas are fabricated, saving a dielectric layer compared to other 5G arrays and improving compactness [19]. Additionally, unlike many of the designs mentioned in Table 1, the proposed antenna stack-up is monolithic, with the superstrate fixed through a bonding film, eliminating the need for air gaps and spacers. The antenna element is a cross-dipole that provides dual linear polarizations. The cross-dipole antennas are widely used in various applications, such as satellite communications [20], [21], mobile communications [22], RFID systems [23], and wireless power transfer [24]. These antennas can provide dual beams and can be arranged to produce a single circularly polarized beam [25]. Cross-dipole antennas have been designed and optimized for operation at low frequency bands, ranging from VHF [24] to S-band [25], in dual polarization [22] or single circular polarization [23], [24], [25]. These antennas offer several advantages, such as a wider

operating frequency band compared to microstrip antennas and the ability to radiate both polarizations through the same element.

The paper is organized as follows. In Section II the general antenna architecture is presented, and it is described by considering all different layers required in the stack-up, with a focus on the choice of the manufacturing technology which drives the design. In Section III the antenna element design is discussed, with a focus on the technical constraints and the adopted solutions. In this section it is analyzed how the layout has been simplified towards the goal of complexity reduction, by eliminating the critical issues which can introduce undesired errors in manufacturing or increase the machining steps, and therefore the costs. Section IV contains the description of the antenna array and a discussion of the constraints in the co-design of both antenna and feeding network. Section V is devoted to the analysis of the performances of both the single element and the entire array, in terms of operative bandwidth, gain and beam steering capabilities. Finally, conclusions are drawn with a comparison with the state of art.

## II. ANTENNA REQUIREMENTS AND ARCHITECTURE

Table 1 presents the main characteristics of the current state-of-the-art array for 5G communications, operating in the mm-Wave frequency band 26.5 – 29.5 GHz. Based on the works in Table 1, the array has to meet the following requirements: i) at least  $\pm 20^\circ$  of steering ability in two main planes, ii) provide 16 – 21 dBi of gain at broadside, iii) exhibit side lobe levels  $< -10$  dB, and iv) have a scan loss  $< 2$  dB [5].

Direct-fed microstrip patch antennas, although compact and robust structures, have a limited BW (1 – 5%) and suffer from losses [4]. Hence, printed cross-dipoles were adopted, and the four dipole arms were shaped to enhance the operative bandwidth. The bandwidth enhancement is achieved by shaping the basic element, resulting in a less technologically demanding stack-up, as opposed to more challenging approaches based on Fabry-Perot cavities [26] or heuristic optimization procedures, such as genetic algorithms and particle swarm optimization as carried out in [13]. The proposed antenna, as shown in Fig. 1 has a minimum number of layers, which simplifies the technological requirements compared to the complex layout found in [9], which requires an air cavity, thus, making it not monolithic. Moreover, no buried vias are involved in the geometry. PCB technology, a low-cost technology, allows for easily drilling of the substrate for the vias with high precision (with a minimum radius  $r$  of 0.150 mm [27]). The metals on the substrates can be printed and shaped independently, and the substrates can then be bonded with a Prepreg resin film. The resulting structure is compact and contains both the radiating system and the feeding network. The choice of adopting the PCB technology for the manufacturing is advantageous due to its low-cost and minimal manufacturing errors, which usually leads to well-matched measured performance with the simulated results. By considering the works presented in

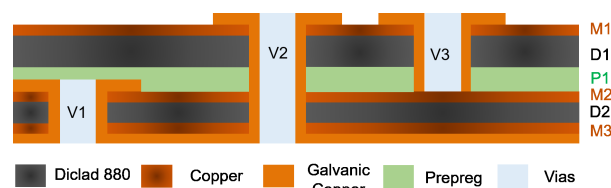


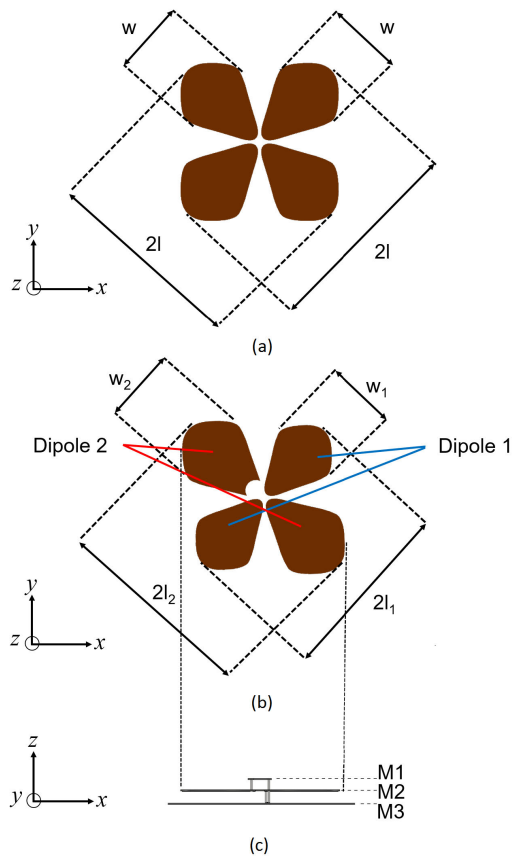
FIGURE 1. Optimized stack-up of the antenna system.

TABLE 2. Summary of the stack-up geometry: antenna layout arrangement.

Layer	Antenna components
D1	Upper dielectric slab (supstrate)
D2	Bottom dielectric slab
M1	Balun for dipole 2
M2	Dipoles and Balun for dipole 1
M3	Feeding Network
P1	Prepreg resin
V1	Feed pin vias, balun vias for dipole 1
V2, V3	Balun vias for dipole 2

Table 1, which were manufactured using PCB technology, we can provide an indication on the accuracy of full-wave simulations. For instance, in [8], the measurements not only confirm the simulated results but even improve them. Similarly, in [11], the simulated and measured Return Loss (RL) and Axial Ratio are well matched. In [12], the measured RL keeps the same worst value calculated by HFSS, and the upper frequency limit is enlarged. In [13], the CST simulation and measurements are well matched, both in the 28 GHz and in the 38 GHz frequency bands. All these works indicate that simulations are reliable for evaluating the real performance of PCB-based mm-wave antennas. In the other works, such as [10], where the design is not PCB-based and non-monolithic, the measured bandwidth is larger than that evaluated with CST Microwave Studio, while the gain value remains constant. Similarly, the multilayer PCB antennas presented in [18] and [19], designed respectively in CST and HFSS, confirm this trend.

The study has been carried out through numerical analyses using CST Microwave Studio (Simulia 3DS, GE). The proposed antenna design consists of two low-losses dielectric laminates, which are placed on top of each other and bonded together with a Prepreg adhesive dielectric film (Fig. 1). The PCB substrate used is Diclad 880 ( $\epsilon_r = 2.2$ ,  $\tan \delta = 0.0009 @ 10$  GHz) [28], with thicknesses of 0.508 mm and 0.787 mm, respectively, for upper and lower layers (D1, D2 in Fig. 1), whereas the Prepreg ( $\epsilon_r = 3.16$ ,  $\tan \delta = 0.0021 @ 10$  GHz) [29] layer (P1) is 0.1 mm thick. The antenna design requires only three metal layers. The radiating part of the system lays in the metal M2, where one of the baluns is also allocated. The metal M1 hosts a bridge required for the realization of the second balun (M1 and vias), which brings the correct potential to the other dipole arms. These two metals are required to split the balun paths on two different levels to avoid undesired crosses and shorts. The



**FIGURE 2.** Top view (a), (b) and cross section (c) of the dipole antenna element. As regards the top view, the ideal, equal and balanced antenna arms shape (a) and final modification due to the baluns (b) are shown: the Dipole 1 (oriented towards North-East) is  $2l_1 \times w_1$  in size, the Dipole 2 (oriented towards North-West) is  $2l_2 \times w_2$  in size, and presents a shaped arm due to the balun path which reaches the superstrate. In the cross section (c), in accordance with Fig. 1, the dipoles lay in the intermediate metallic layer M2, whereas balun of the Dipole 2 crosses the entire structure until the top layer M1, and reconnect with the proper dipole arm. The level M3 hosts the feeding network. In this view the dielectric layers are neglected.

symmetry (and orthogonality) of the paths ensures reduced coupling between the two radiating elements. The bottom metallic layer (M3) is dedicated to the feeding network, which is realized in coplanar waveguide (CPW). The feeding tracks are connected to the dipoles through metallic vias. One advantage of using CPW for the feeding network is that it needs only a metal layer for its implementation. This design choice eases the whole system integration, compactness, and array arrangement. However, the CPW widths are constrained by the technological limitations of the PCB technology. Therefore, we considered a minimum conductive track width of 0.15 mm and a minimum gap width of 0.20 mm. Table 2 summarizes the stack-up, shown in Fig. 1. In the next section, the array design will be discussed.

### III. ANTENNA DESIGN

In Section II, we discussed the requirements for the radiating system, including dual linear polarization,

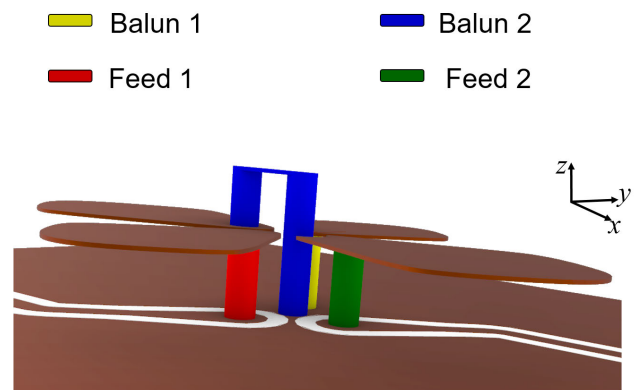


**FIGURE 3.** Antenna element: isometric view of the schematic in Fig. 2. The vias and the baluns are highlighted in different colors.

a bandwidth  $> 1$  GHz centered at 27 GHz, good beam steering capability, and mutual isolation between polarizations. To design the antenna array meeting these requirements, the first step is to choose a unit cell. Several prototypes have been proposed to address the dual polarization issue, including square patches [27], cross-dipoles [30], and interdigitated configurations consisting of two single polarized antennas [31]. Although microstrip patches have a simple dual polarization arrangement, they are typically narrowband. To overcome this limitation, stacked configurations can be used, but this complicates device manufacturing due to air gap tolerances [26]. In contrast, a printed dipole provides a wide frequency band with a single layer geometry, and its array arrangement is not problematic, similar to patch antennas. The radiated beam of a printed dipole guarantees a wide beam steering operation in the array arrangement. Furthermore, the dipoles can be shaped as cross-dipoles, consisting of two dipoles placed orthogonally, creating an array element with two antennas radiating both the horizontal (H) and vertical (V) polarizations. This solution is space-saving compared to interdigitated antenna arrays [31].

For these reasons, in this work we have selected a printed cross dipole as the antenna element due to its ability to expand the bandwidth without affecting impedance matching, as shown in Fig. 2(a). The dipoles consist of two pairs of arms placed orthogonally to each other. The boundary of the patches is optimized via spline curves, with the shape gradually enlarge towards the termination to enhance the operative bandwidth. However, the increase in size is constrained by the mutual coupling between the dipoles within the antenna unit cell, which is greater for bulkier geometries than standard linear dipole antennas. We will refer to Dipole 1 as the antenna element with the balun at the dipole arms level and Dipole 2 as the antenna element with the balun crossing the superstrate and lying on the top metallic layer M1, requiring a cut in one of the conductor arms. The asymmetry in the electric paths that feed the two linear polarizations is also reflected in an asymmetry in the size

of the two dipoles: Dipole 1 is  $2l_1$  long and  $w_1$  wide, while Dipole 2 is  $2l_2$  long and  $w_2$  wide, as shown in Fig. 2(b). The sub-arrays, whose performance is analyzed in section V, are named similarly to their respective dipole antennas. Section II highlights the importance of evaluating the technological aspects and ease of manufacturing processes to reduce overall costs for high frequency applications such as the FR2 5G frequency band. This needs a thorough investigation of antenna solutions that minimize the number of layers and types of vias between them, depending on the kind of vias that connect different pairs of metal layers. One of the simplest antenna geometries is composed of two dipoles and a network of metal connections between them and the level  $M_i$ , which feeds the antennas and connects them to the ground. In the crossed configuration, the balun cross-over horizontal paths have to be arranged on different layers, thus requiring an additional metal layer compared to the stack-up in Fig. 1. To simplify the design complexity and minimize the number of metallic layers and via types, the antenna stack-up can be modified by removing the network of crossed conductors between the lowest metal level and the patches. This also eliminates buried vias, which would introduce several issues, such as separating the machining process into more steps [17], and criticalities in PCB alignment. A non-perfect alignment of the laminates in the stack could affect the correct arrangement of the conductive paths necessary to feed the dipoles, which is avoided with this modified stack-up design. It is worth noting that the absence of buried vias also simplifies the manufacturing process, in contrast to the layout reported in [9]. To mitigate critical issues in manufacturing that can arise due to buried vias, the chosen approach was a stacked architecture with a superstrate hosting the antennas on top (Fig. 1 and Fig. 2(c)). In this design, one balun was shifted to the top layer M1, while the dipoles were realized in layer M2. By placing the lower balun path at the M2 level, the stack-up required only 3 metal layers, with the upper laminate having only one metal. The upper balun was positioned on the top level M1, supported by the upper dielectric slab D1. Together with the prepreg layer P1, D1 acted as a superstrate on the dipoles. The configuration with three metals contained only passing vias, which contacted at least one of the M1, M3 levels (V1, V3), or both (V2) (as shown in Figs. 2(c) and 3. This approach simplified the design, reduced manufacturing costs, and did not affect the radiating properties of the antenna, thanks to the thin and low-loss superstrate. All drillings could be performed after the layers bonding, eliminating potential alignment issues. However, the presence of metallic connections necessitated modifications to the ideal dipole layout (Fig. 2(a)). The via V2, which together with V3 and M1 forms the balun of Dipole 2, required a cut in the arm of Dipole 2 to avoid a short between them, as shown in Fig. 2(b). Moreover, the choice of a layout with a superstrate, as opposed to a more conventional stack-up that hosts the antennas on top, resulted in a very compact antenna in terms of profile height (see Table 1). A top view of the  $4 \times 4$  dipole array is shown in

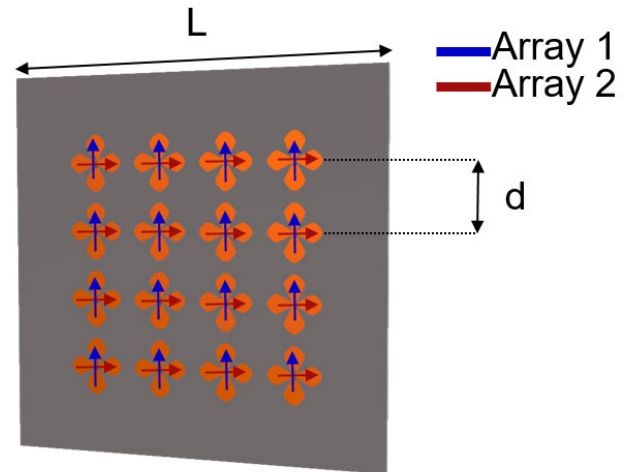


**FIGURE 4.** Top view of the  $4 \times 4$  dipole array. The superstrate and the prepreg layers are not displayed for a sake of clarity. The current distributions of the two polarizations are highlighted in blue (Array 1) and red (Array 2).

Fig. 4, where the current distributions of the two polarizations are highlighted in blue (Array 1) and red (Array 2).

#### IV. ARRAY ARRANGEMENT

The antenna element discussed above is used as unit cell in the complete array. The array comprises  $4 \times 4$  elements (Fig. 4, where the upper dielectric slabs are not drawn for simplicity of visualization), with 32 dipoles, 16 for each polarization. The complexity of the array, along with the technology constraints for the antenna and feeding network, imposes limitations on the minimum distances between the elements. These distances permit allocation of all the conductive tracks without shorting them to the antenna vias while also keeping a low coupling among the tracks to prevent undesired energy coupling. The minimum conductor width of 0.15 mm and a minimum air gap of 0.2 mm, which are dictated by the adopted PCB technology, must be respected. Given these limitations, the minimum distance between the array elements is set to  $d = 7$  mm, equal to  $0.63\lambda_0$  at 27 GHz (Fig. 4). This distance is acceptable for grating lobe prevention, considering the scanned angular range. The upper dielectric slabs are not shown in Fig. 4 for simplicity of visualization.

#### A. FEEDING SYSTEM

The feeding network is strongly connected to the array arrangement as it is responsible for providing all the array elements with the correct amplitude and phase distributions required to steer the beam towards the desired direction. As aforementioned in Section II, the network is hosted on the bottom M3 metal layer and consists of a suitably designed CPW network. The frequency involved leads to a high antenna density (about 8 per square centimeter, 4 per each polarization), which makes it difficult to place a set of coaxial connectors directly on the bottom of the PCB.

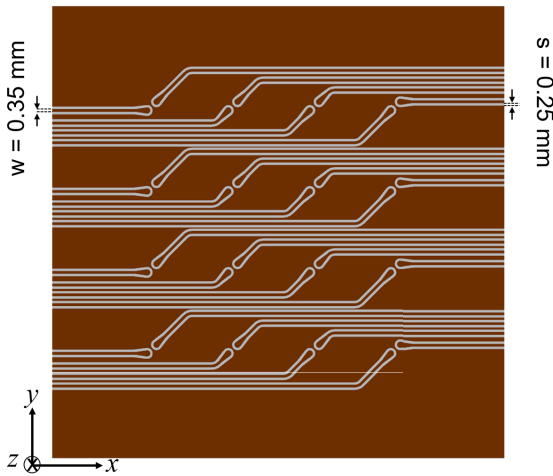


**FIGURE 5.** Feeding network. The CPW network reports all the tracks relative to the same polarization on the same side, where they will be connected to a set of phase shifters.

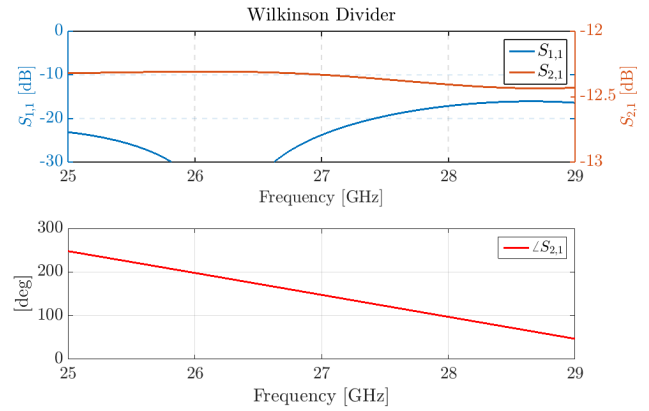


**FIGURE 7.** CPW Wilkinson divider network for one linear polarization; S-parameters between the ports 1 and 2 (see Fig. 6).

**TABLE 3.** Cross dipole dimensions.

	$2l_1$	$w_1$	$2l_2$	$w_2$
[mm]	5.2	1.8	5.7	2

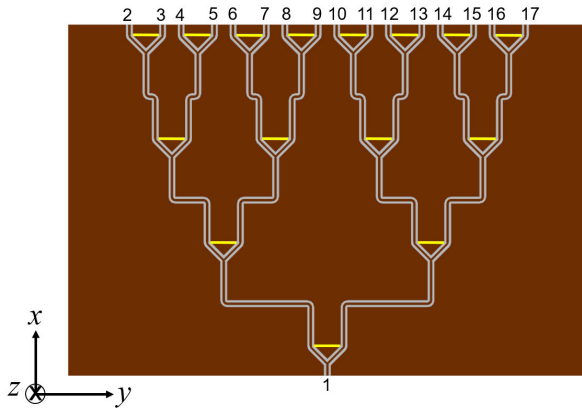


**FIGURE 6.** Feeding network. CPW Wilkinson divider network for one linear polarization. The yellow lines represent the resistors.

Given these technological limitations, it is advantageous to define a network of conductive tracks that separates the feeds of the two subarrays and brings the electric paths of all antennas with the same polarization to the same board side. The feeding network consists of two main parts: the network under the array, which connects the strips on the array sides (Fig. 5), and the network that combines the tracks of each polarization to connect to the common feeding connector (Fig. 6).

The array period  $d$ , in combination with the CPW traversal size, is the parameter which mostly constrained the overall network design. Moreover, the vias shorted to M3 in addition to the feeding vias (e.g., the baluns) should not overlap the conductive tracks, so that an additional constraint in the feeding network design is introduced. Fig. 5 shows the CPW network layout, which is placed in the array back-side to properly feed each dipole antenna according to its appropriate polarization. This metal layer (M3) acts in the

same time as a ground plane for the dipoles, which radiate in its presence. The dimensions are respectively  $w = 0.35$  mm,  $s = 0.25$  mm for the conductive strips and the gaps widths, with an impedance equal to  $100 \Omega$ . The second part of the network is build-up through a tree of Wilkinson dividers (16-to-1 circuit) per each polarization, the Wilkinson Divider Network (WDN), and it is shown in Fig. 6. The phase distribution is provided to each dipoles sub-array via a set of CPW delay lines applied to the network, which allows to compensate the phase delays due to the unequal length of the tracks (Fig. 5) and to steer the beam in the desired angle. The resulting scattering parameters for the WDN are shown in Fig. 7. In this graph, it is reported the  $S_{21}$ , between the port 2 and the port 1, which is  $-12.33$  dB in magnitude at 27 GHz, as it is expected for a 16 output ports power divider, whereas the  $S_{11}$  at the input port 1 stands under  $-20$  dB at 27 GHz and under  $-17$  dB in the frequency band 26-28 GHz. The phase distribution to be provided to the two dipole sub-arrays is arranged via a set of phase shifters applied to the network, downstream the power divider, which allows to steer the beams in the desired angles.

**V. RESULTS**

In this section, the simulated results of the designed antenna are presented. First, the antenna element has been tested alone, in terms of scattering parameters and radiated fields. After, the array performances have been evaluated.

**A. ARRAY UNIT CELL**

Due to the different balun lengths, the size of the two dipoles (see Fig. 2(b)) is different (the optimized dimensions are reported in Table 3).

The resulting scattering parameters are shown in Fig. 8. The crossed dipoles show a good impedance matching (i.e.,

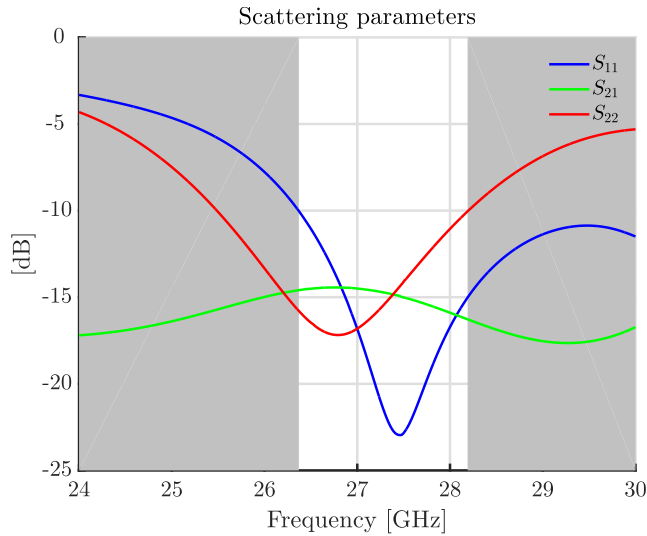


FIGURE 8. Scattering parameters for the cross dipole.

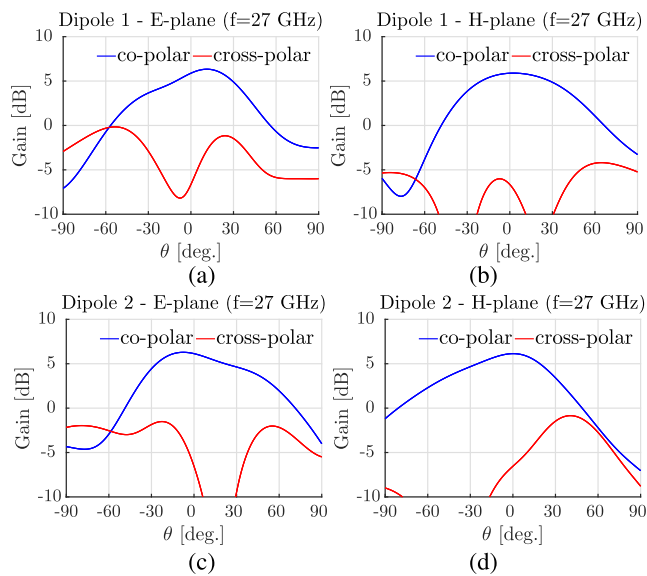


FIGURE 9. Far field radiation performance of the antenna: for each antenna it is represented the Gain in terms of components on the E- and H- planes.

maximum return loss of respectively 22 dB and 17 dB for dipoles 1 and 2, see Fig. 2), the available BW for both the dipoles is 1.82 GHz @ 27.28 GHz (26.37 - 28.19 GHz), whereas the mutual coupling between them is less than -14 dB in such a frequency band. Even this value is not very high, it is comparable with other dual polarized antennas proposed for mm-wave 5G [33], and obtained with a low-cost layout. The BW is around 7%, better than the PCB-based works in [8], [10], [11], and [13]. The far field of the two dipoles is shown in Fig. 9. The maximum co-polar gains at 27 GHz are respectively 6.25 dB and 6.31 dB for the dipoles 1 and 2. The slight unequal main lobe direction (about 6 degrees for both the antennas) is due to the parasitic effect of each antenna (dipole arms and baluns) on the other

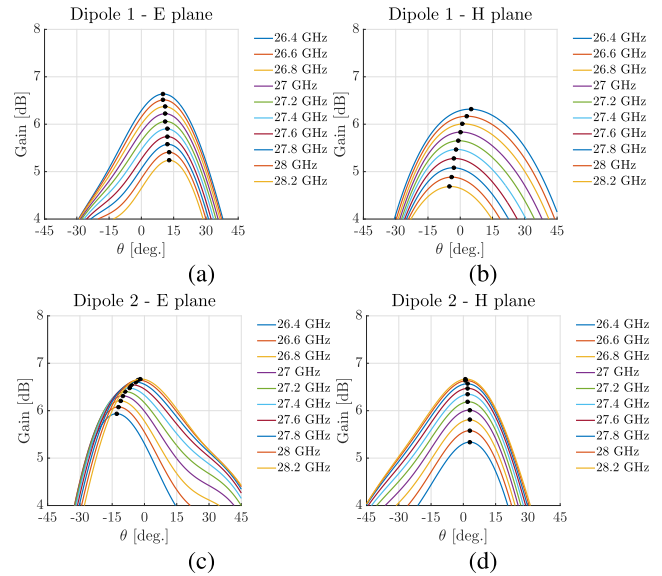


FIGURE 10. Far field radiation performance of the antennas over frequency: for each antenna it is represented the Gain in terms of the co-polar component on the E- and H- planes. The black dots highlight the maxima.

one, but it is small enough to not affect the array operation significantly. The cross-polar component is 10 dB lower than the co-polar in broadside direction for both the dipoles in both the cut-planes ( $\phi = 0^\circ$  and  $\phi = 90^\circ$ ), as it can be observed in Fig. 9.

In Fig. 10 a study of the farfield performance over frequency is reported. As in Fig. 9, both the E- and H-plane are displayed for both the dipoles. Even if the main lobe radiation appears to be affected by a notable drift, the gain value does not vary sensibly, therefore, in the array arrangement this drift will be compensated. In effect, the beam is wide enough such that the “gain loss” between the main lobe direction and the broadside is not very sensible: at 27 GHz, this loss is 0.55 dB for Dipole 1 and 0.92 dB for Dipole 2.

### B. ANTENNA ARRAY

The antenna elements are arranged in a bi-dimensional array (as shown in Fig. 4) with a 7 mm inter-element distance. The proposed configuration, with a stable gain for both the linear polarizations, is expected to offer a beam scanning angular range comparable with the state of art solutions reported in Table 1.

Fig. 11 shows the far field radiation pattern for both the sub-arrays. The Gain at 27 GHz is 15.90 dB for the dipole Array 1 (Fig. 11(a)) and 15.98 dB for dipole Array 2 (Fig. 11(b)), and the side lobe levels are, respectively, -16.05 dB and -14.10 dB. In both the polarizations, the cross-polar component is more than 10 dB lower than the co-polar.

To evaluate the performance over the operative frequency band, Fig. 12 displays the co-polar gain over frequency

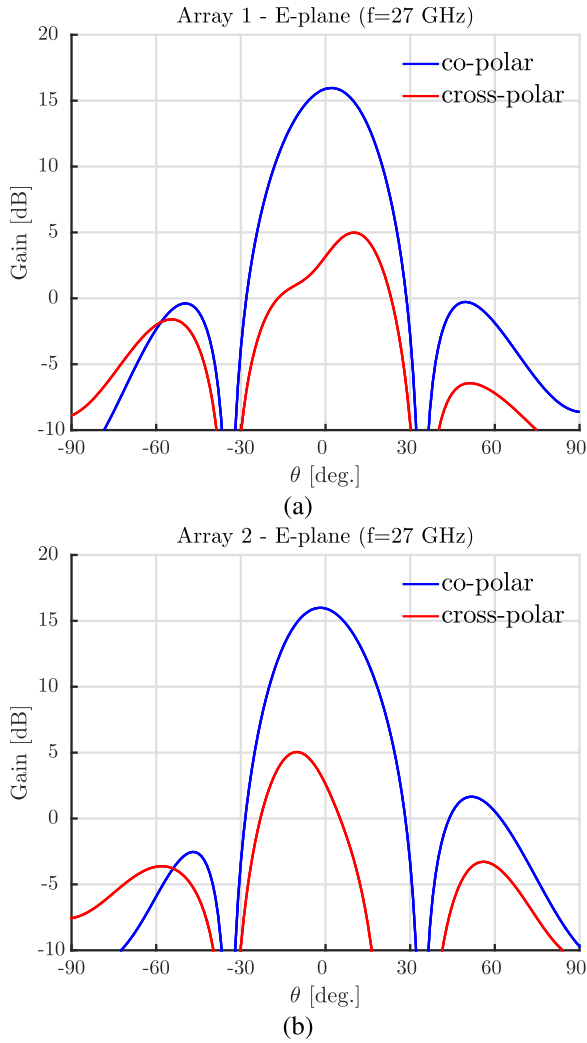


FIGURE 11. Far field of the antenna sub-arrays 1 (a) and 2 (b) (broadside radiation).

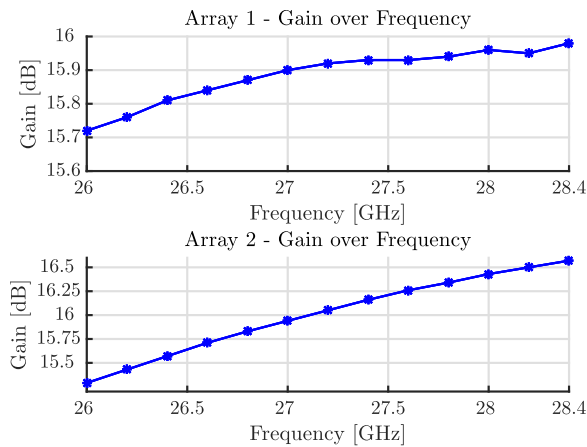


FIGURE 12. Broadside gain of the dipole Arrays 1 (top) and 2 (bottom) over the frequency.

for the two dipole arrays: they keep its value in the range 15.72 – 15.98 dB (Array 1) and 15.29 – 16.57 dB (Array 2)

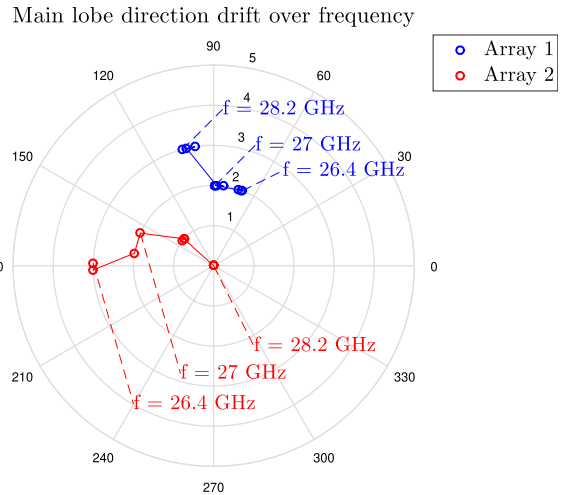


FIGURE 13. Main lobe direction drift over the frequency of the dipole Arrays 1 (blue) and 2 (red). In the polar graph, the radial dimension is the elevation angle (plot from broadside to 5 degrees), whereas the azimuth angle is plot for  $(0,2\pi)$ .

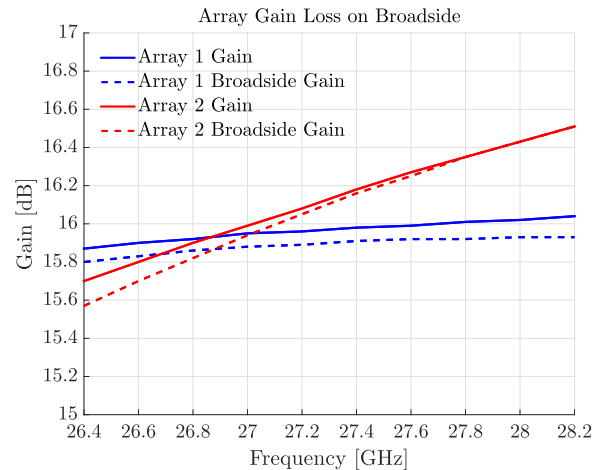
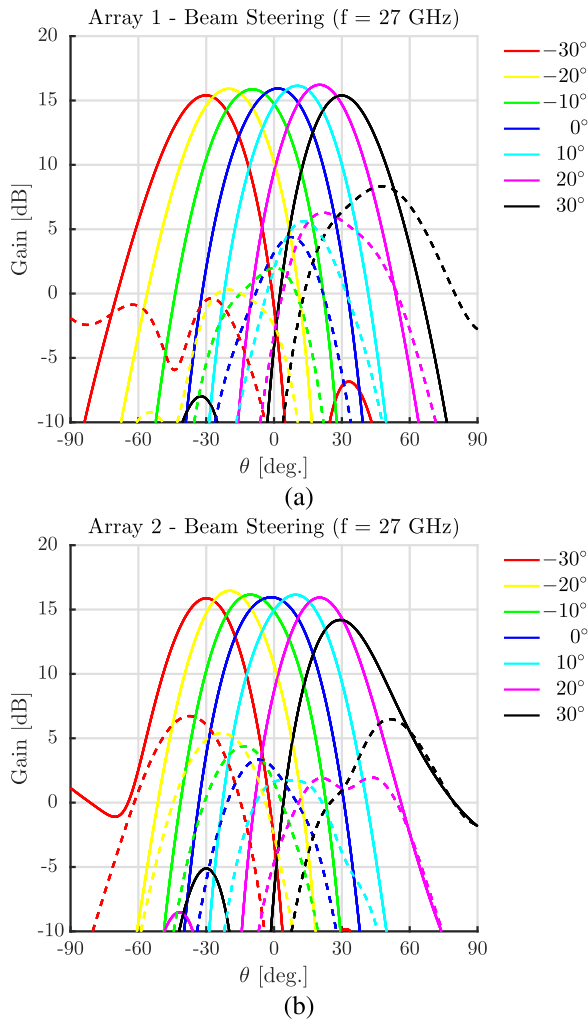


FIGURE 14. Gain loss between the main lobe direction (solid line) and broadside (dashed line) for the Arrays 1 (blue) and 2 (red) over the frequency.

between 26 and 28.4 GHz. This result further validates the antenna functionality. Since the main lobe direction of the single antenna element is affected by a noticeable drift over the frequency, but with a low gain loss between this direction and broadside, it is important to evaluate how this is compensated by the Array arrangement. This can be appreciated in Fig. 13: both the array beams keep their elevation angle inside a 3 degrees out of the broadside direction for the whole operative frequency band. To understand how this affects the broadside gain performance of the Array, in Fig. 14 are plotted, for both the Arrays, the Gain and the Broadside Gain. It can be appreciated how the difference between them is less than 0.2 dB for both the polarizations in the whole frequency band.

The radiation efficiency at 27 GHz is respectively 93% and 94% for dipole Arrays 1 and 2, with a 3% difference from the results obtained by the  $4 \times 4$  patch array characterized in [11].





**FIGURE 15.** Far field of the antenna sub-arrays: beam steering performance for antenna Array 1 (a) and 2 (b). (Solid line: copolar component; dashed line: crosspolar component). Tables 4, 5 list the detailed performance.

By considering the area occupied by the arrays, the maximum available gains at 27 GHz are 17.84 dB for the Array 1 and 17.96 dB for Array 2, which reflect in an aperture efficiency equal respectively to 63.99% and 62.24% [32].

Since one of the main appealing features in 5G arrays is the beam steering capabilities [5], [10], [12], the dipole arrays have been tested along their equatorial planes ( $\phi = 0^\circ$ ). Fig. 15 presents the beam steering performance for steering angles up to  $30^\circ$ , which is a value higher than the recommendation reported in [5] and outperforms the results in [10] and [12]. In both Array 1 and Array 2, the gain does not decrease sensibly over the whole angular range (the gain degrades up to 2 dB and the side lobe level keeps low, under  $-15$  dB). The cross-polar component keeps more than 10 dB lower with respect to the co-polar until 20 degrees scanning angle. It is worth noting that the asymmetric positions of the vias affect the beam steering capability of the Array 2. Tables 4 and 5 summarize overall performance. These beam steering capabilities, combined with the almost stable

**TABLE 4.** Beam steering performance for Array 1.

	Unit	Value			
Phase shift	[deg.]	0	18	42	68
Gain	[dB]	15.9	16.1	16.2	15.4
MLD	[deg.]	0	10	20	30
AW	[deg.]	30	28.6	27.5	27.4
SLL	[dB]	-19	-20.3	-19.5	-18

MLD = Main Lobe Direction, AW = Angular Width, SLL = Side Lobe Level

**TABLE 5.** Beam Steering performance for Array 2.

	Unit	Value			
Phase shift	[deg.]	0	20	47	72
Gain	[dB]	16	16.1	15.9	14
MLD	[deg.]	0	10	20	30
AW	[deg.]	32.3	29	26.7	27.9
SLL	[dB]	-22.2	-17	-23	-16.9

MLD = Main Lobe Direction, AW = Angular Width, SLL = Side Lobe Level

gain, hint the suitability of the antenna for mm-Wave 5G applications.

### C. DISCUSSION

As reported in Table 1, the proposed antenna results to be low profile (1.60 mm), being less cumbersome than the LWA lens array in [5], the dielectric resonator in [8], the  $8 \times 8$  array of patch antennas fed by aperture coupling in [9], the  $4 \times 4$  array in SIW technology in [10] and the optimized patch array presented in [11]. In terms of size, the designed antenna occupies less space than the solutions reported in [5], [10], [11], and [13].

The antenna provides a dual linearly polarized radiated field, with an impedance BW larger than 1.8 GHz ( $\sim 7\%$ ). The BW is comparable to that reported by [8] for the DDR linear array, whilst is about 1.45 times higher than the BW of the SIW  $4 \times 4$  dipoles array [10] and the patch array from [11]. On the other hand, the BW is narrower compared with the 5G arrays from [5], [9], and [12]. The antenna array has a maximum gain of 16 dBi, which is higher than that reported for the  $4 \times 4$  patch array from [11], but it is comparable to the gain values of the arrays from [8] and [10], while being  $\sim 17\text{-}35\%$  lower than the values reported in [5], [9], and [12]. The radiation efficiency is  $\sim 93\%$  for both the polarizations, similar to the performance presented in [10], but with a wider bandwidth. Our array, with the designed feeding network, demonstrated a scanning angle of  $\pm 30^\circ$ , which is a better performance than the arrays in [5], [10], and [12]. The isolation between the two polarizations is around 15 dB, and even if it is not very high, is similar to other dual polarized antennas operating in similar frequency bands [33], where the experimental measurement confirmed the simulated performance.

It is worth noting that the main lobe squint is due, most of all, to the asymmetry in the geometry, that is the different circuitry which surrounds the two dipole elements. The main responsible of this issue is the balun path which crosses

the stack-up till level M1. Anyway, this main lobe direction drift is alleviated by the array arrangement, as displayed in Fig. 13, and the gain loss in the broadside direction is not very high (see Fig. 14). A stack-up with all the baluns placed under the radiating element would reduce this effect but it would increase the manufacturing issue and therefore the costs. Therefore, this result is an acceptable trade-off between the farfield radiation performance and the constructive complexity.

Although the array has been proposed only with simulated results, we are confident on the performance evaluated by the electromagnetic simulation software, as evinced by the results presented in the references in Table 1 and analysed in Section II as State of art. As well as such results in the table, several works show how the level of accuracy of the modern simulators allows to consider reliable the simulated results, especially in simple geometries as the PCB layout we propose. In [33], a dual-polarized millimeter-wave patch antenna array is proposed, with an insulation value comparable with our work, such a value is almost the same in simulation and experimental measurement, with a slight improvement in the second case. In [34], an antenna manufactured in PCB laminates is presented, and the degradation between simulation and experiment in the RL is around 3dB at 27.5 GHz, this does not compromise the antenna operation. The same applies to other 5G antenna based on other technologies, as [35] and [36], where the measurement keeps the performance evaluated in simulation. In [37], a multilayer array antenna operating in E band is proposed, the complexity of the system does not reflect on the discrepancy between simulated and measured results, and the device keeps in the RL measurement almost the same performance evaluated in the simulation step, up to 85 GHz. In the Return Loss, there is a slight bandwidth reduction (10%) in the low frequencies between measurement and simulations, a very accurate matching in central frequencies (the worsening is less than 5dB with a nominal simulated value higher than 17 dB), and a small deviation over 80 GHz which does not compromise the operation, as the upper frequency limit. These results encourage the development of the proposed antenna array for 5G mm-Wave communication systems.

## VI. CONCLUSION

In this work, we designed a cross-dipole array antenna for 5G mm-Wave applications which outperforms the available solutions in terms of scanning angle, profile height and size, while retaining BW and gain values comparable to the state of the art mm-Wave arrays (see Table 1). The antenna design has been oriented to make its manufacturing suitable for the PCB technology, with a particular attention to the fabrication cost reduction. With this goal, the stack-up complexity has been drastically reduced with respect to other available solutions: the feeding network and antenna conductors lay on the same DiClad 880 laminate, as well as one of the baluns. The upper laminate is used to shape the

second balun path, and its bottom metallic layer is completely removed. The main feature introduced in the stack-up, linked to the number of layers reduction, is its rearrangement to avoid the usage of internal vias. All the vias which connect the different components reach the top or the bottom of the stack-up, therefore they do not add intermediate manufacturing steps, which introduce potential sources of errors and, indeed, additional costs. The integration of the feeding network in the same laminate which hosts the antenna, through the use of CPW transmission lines, increases the compactness of the device. These technological choices contribute to reduce the complexity of the stack-up, in terms of number of layers and metallic vias, thus they make the design simpler and cheaper.

Although the antenna arrangement has been deeply driven by the search of the easiest constructive complexity, which led also to a very reduced thickness, the antenna performance keeps competitive with the state of art: a bandwidth of 1.82 GHz @ 27.28 GHz, around 7% in percentage terms, together with a scanning angle of  $\pm 30^\circ$  lay inside the value commonly provided by 5G antennas, as it can be evaluated from Table 1.

## ACKNOWLEDGMENT

(Marco Simone and Santi Concetto Pavone contributed equally to this work.)

## REFERENCES

- [1] W. H. Chin, Z. Fan, and R. Haines, "Emerging technologies and research challenges for 5G wireless networks," *IEEE Wireless Commun.*, vol. 21, no. 2, pp. 106–112, Apr. 2014.
- [2] E. Liu, E. Emmanuel, and J. Hitchcock, "Survey on health care applications in 5G networks," *IET Commun.*, vol. 14, no. 7, pp. 1073–1080, 2020.
- [3] V. Ilderem, "The technology underpinning 5G," *Nat. Electron.*, vol. 3, no. 1, pp. 5–6, 2020.
- [4] H. Ozpinar, S. Aksimsek, and N. T. Tokan, "A novel compact, broadband, high gain millimeter-wave antenna for 5G beam steering applications," *IEEE Trans. Veh. Technol.*, vol. 69, no. 3, pp. 2389–2397, Mar. 2020.
- [5] H. Zhang, S. Bosma, A. Neto, and N. Llombart, "A dual-polarized 27 dBi scanning lens phased array antenna for 5G point-to-point communications," *IEEE Trans. Antennas Propag.*, vol. 69, no. 9, pp. 5640–5652, Sep. 2021.
- [6] M. Li, M. Y. Jamal, C. Zhou, L. Jiang, and L. K. Yeung, "A novel dipole configuration with improved out-of-band rejection and its applications in low-profile dual-band dual-polarized stacked antenna arrays," *IEEE Trans. Antennas Propag.*, vol. 69, no. 6, pp. 3517–3522, Jun. 2021.
- [7] B. Yu, K. Yang, C.-Y.-D. Sim, and G. Yang, "A novel 28 GHz beam steering array for 5G mobile device with metallic casing application," *IEEE Trans. Antennas Propag.*, vol. 66, no. 1, pp. 462–466, Jan. 2018.
- [8] O. M. Haraz, A. Elboushi, S. A. Alshebeili, and A. R. Sebak, "Dense dielectric patch array antenna with improved radiation characteristics using EBG ground structure and dielectric superstrate for future 5G cellular networks," *IEEE Access*, vol. 2, pp. 909–913, 2014.
- [9] X. Gu, D. Liu, C. Baks, O. Tageman, B. Sadhu, J. Hallin, and L. Rexber, "Development, implementation, and characterization of a 64-element dual-polarized phased-array antenna module for 28-GHz high-speed data communications," *IEEE Trans. Microw. Theory Techn.*, vol. 67, no. 7, pp. 2975–2984, Jul. 2019.
- [10] M. Asaadi and A. Sebak, "High-gain low-profile circularly polarized slotted SIW cavity antenna for MMW applications," *IEEE Antennas Wireless Propag. Lett.*, vol. 16, pp. 752–755, 2017.
- [11] E. Al Abbas, N. Nguyen-Trong, A. T. Mobashsher, and A. M. Abbosh, "Polarization-reconfigurable antenna array for millimeter-wave 5G," *IEEE Access*, vol. 7, pp. 131214–131220, 2019.

- [12] C.-X. Mao, S. Gao, and Y. Wang, "Broadband high-gain beam-scanning antenna array for millimeter-wave applications," *IEEE Trans. Antennas Propag.*, vol. 65, no. 9, pp. 4864–4868, Sep. 2017.
- [13] K. R. Mahmoud and A. M. Montaser, "Synthesis of multi-polarised upside conical frustum array antenna for 5G mm-Wave base station at 28/38 GHz," *IET Microw., Antennas Propag.*, vol. 12, no. 9, pp. 1559–1569, Jul. 2018.
- [14] S. C. Pavone, M. Casaletti, and M. Albani, "Automatic design of a CP fan-beam linear slotted array in SIW technology," *IEEE Access*, vol. 7, pp. 155977–155985, 2019.
- [15] M. Ettorre, S. C. Pavone, M. Casaletti, M. Albani, A. Mazzinghi, and A. Freni, "Near-field focusing by non-diffracting Bessel beams," in *Aperture Antennas for Millimeter and Sub-Millimeter Wave Applications*. Cham, Switzerland: Springer, pp. 243–288, 2018.
- [16] S. C. Pavone, E. Martini, M. Albani, S. Maci, C. Renard, and J. Chazelas, "A novel approach to low profile scanning antenna design using reconfigurable metasurfaces," in *Proc. Int. Radar Conf.*, 2014, pp. 1–4.
- [17] T. Potelon, M. Ettorre, L. Le Coq, T. Bateman, J. Francey, and R. Sauleau, "Reconfigurable CTS antenna fully integrated in PCB technology for 5G backhaul applications," *IEEE Trans. Antennas Propag.*, vol. 67, no. 6, pp. 3609–3618, Jun. 2019.
- [18] I. L. de Paula, S. Lemey, D. Bosman, Q. Van den Brande, O. Caytan, J. Lambrecht, M. Cauwe, G. Torfs, and H. Rogier, "Cost-effective high-performance air-filled SIW antenna array for the global 5G 26 GHz and 28 GHz bands," *IEEE Antennas Wireless Propag. Lett.*, vol. 20, no. 2, pp. 194–198, Feb. 2021.
- [19] A. Lamminen, J. Säily, J. Ala-Laurinaho, J. de Cos, and V. Ermolov, "Patch antenna and antenna array on multilayer high-frequency PCB for D-band," *IEEE Open J. Antennas Propag.*, vol. 1, pp. 396–403, 2020.
- [20] L. Wang, H.-C. Yang, and Y. Li, "Design of a new printed dipole antenna using in high latitudes for Inmarsat," *IEEE Antennas Wireless Propag. Lett.*, vol. 10, pp. 358–360, 2011.
- [21] H. Govindarajan, S. C. Pavone, L. D. Donato, P. D. Mariano, and G. Distefano, "Design of a compact dual circular-polarized antenna for L-band satellite applications," *IEEE Antennas Wireless Propag. Lett.*, vol. 19, no. 4, pp. 547–551, Apr. 2020.
- [22] K. M. Mak, H. Wong, and K. M. Luk, "A shorted bowtie patch antenna with a cross dipole for dual polarization," *IEEE Antennas Wireless Propag. Lett.*, vol. 6, pp. 126–129, 2007.
- [23] H.-M. Chen, Y.-K. Wang, Y.-F. Lin, and Z.-Z. Yang, "Single-layer crossed dipole antenna with circular polarization for handheld RFID reader," *Microw. Opt. Technol. Lett.*, vol. 53, no. 5, pp. 1172–1176, 2011.
- [24] I.-J. Yoon and H. Ling, "Design of an electrically small circularly polarised turnstile antenna and its application to near-field wireless power transfer," *Microwaves, Antennas Propag.*, vol. 8, no. 5, pp. 308–314, Apr. 2014.
- [25] Y. Feng, J. Li, B. Cao, J. Liu, G. Yang, and D. J. Wei, "Cavity-backed broadband circularly polarized cross-dipole antenna," *IEEE Antennas Wireless Propag. Lett.*, vol. 18, no. 12, pp. 2681–2685, Dec. 2019.
- [26] M. Simone, A. Fanti, and G. Mazzarella, "5G wideband stacked patch antennas," in *Proc. 15th Eur. Conf. Antennas Propag. (EuCAP)*, 2021, pp. 1–5.
- [27] T. Chaloun, V. Ziegler, and W. Menzel, "Design of a dual-polarized stacked patch antenna for wide-angle scanning reflectarrays," *IEEE Trans. Antennas Propag.*, vol. 64, no. 8, pp. 3380–3390, Aug. 2016.
- [28] Rogers Corporation. *DiClad Series® Data Sheet*. Accessed: Mar. 30, 2023. [Online]. Available: <https://rogerscorp.com/-/media/project/rogerscorp/documents/advanced-connectivity-solutions/english/data-sheets/diclad-series-data-sheet.pdf>
- [29] Rogers Corporation. *SpeedWave<sup>®</sup> 300P Prepreg*. Accessed: Mar. 30, 2023. [Online]. Available: <https://rogerscorp.com/-/media/project/rogerscorp/documents/advanced-electronics-solutions/english/data-sheets/speed-wave-300p-data-sheet.pdf>
- [30] S. X. Ta, I. Park, and R. W. Ziolkowski, "Crossed dipole antennas: A review," *IEEE Antennas Propag. Mag.*, vol. 57, no. 5, pp. 107–122, Oct. 2015.
- [31] W. Hong, K.-H. Baek, and S. Ko, "Millimeter-wave 5G antennas for smartphones: Overview and experimental demonstration," *IEEE Trans. Antennas Propag.*, vol. 65, no. 12, pp. 6250–6261, Dec. 2017.
- [32] C. A. Balanis, *Antenna Theory: Analysis and Design*, 3rd ed. Hoboken, NJ, USA: Wiley, 2005, pp. 653–738.
- [33] Y. He, S. Lv, L. Zhao, G.-L. Huang, X. Chen, and W. Lin, "A compact dual-band and dual-polarized millimeter-wave beam scanning antenna array for 5G mobile terminals," *IEEE Access*, vol. 9, pp. 109042–109052, 2021.
- [34] T. Deckmyn, M. Cauwe, D. V. Ginste, H. Rogier, and S. Agneessens, "Dual-band (28,38) GHz coupled quarter-mode substrate-integrated waveguide antenna array for next-generation wireless systems," *IEEE Trans. Antennas Propag.*, vol. 67, no. 4, pp. 2405–2412, Apr. 2019.
- [35] X. Gu, "Antenna-in-package integration for a wideband scalable 5G millimeter-wave phased-array module," *IEEE Microw. Wireless Compon. Lett.*, vol. 31, no. 6, pp. 682–684, Jun. 2021.
- [36] S. X. Ta, H. Choo, and I. Park, "Broadband printed-dipole antenna and its arrays for 5G applications," *IEEE Antennas Wireless Propag. Lett.*, vol. 16, pp. 2183–2186, 2017.
- [37] Z. S. He, C. Jin, S. An, L. Kong, and J. Liu, "Integrated-EBG ridge waveguide and its application to an E-band waveguide 32×32 slot array antenna," *IEEE Open J. Antennas Propag.*, vol. 1, pp. 456–463, 2020.



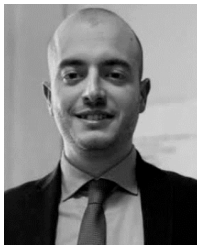
**MARCO SIMONE** received the master's degree in electronic engineering and the Ph.D. degree in electronic and computer engineering from the University of Cagliari, Italy, in 2011 and in 2016, respectively. He was a visiting Ph.D. student with the Queen Mary University of London (QMUL), London, U.K., in 2015, where he was a Postdoctoral Research Assistant with the Antennas & Electromagnetics Research Group, in 2016 and 2017. Since 2017, he has been an Associate Researcher with the Laboratory of Applied Electromagnetics, University of Cagliari. His research interests include optimization techniques applied to electromagnetics problems, microwave components design for radioastronomy applications, and antenna design.



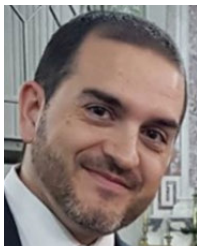
**SANTI CONCETTO PAVONE** (Senior Member, IEEE) received the B.Sc. and M.Sc. degrees (summa cum laude) in electronics engineering from the University of Messina, Messina, Italy, in 2010 and 2012, respectively, and the Ph.D. degree (with the additional label of Doctor Europaeus) in information engineering and science (electromagnetics engineering) from the University of Siena, Siena, Italy, in 2015. He was a visiting Ph.D. student and an Assistant Professor with Institut d'Électronique et de Télécommunications de Rennes, Université de Rennes 1, Rennes, France, in 2015 and 2020, respectively. From 2016 to July 2019, he was an Associate Researcher with the Laboratory of Applied Electromagnetics, University of Siena. Since August 2019, he has been an Assistant Professor with the Department of Electrical, Electronics, and Information Engineering, University of Catania, Italy. His current research interests include fundamental electromagnetic theory, scattering theory, RADAR design at millimeter waves, high-frequency techniques, focusing systems, nondiffractive localized pulses, and reconfigurable antennas. He was a recipient of the ESF Research Networking Programme NEWFOCUS Scholarship, in 2015, and the IEEE Antennas and Propagation Society Student Award, Chapter Central-Southern Italy, in 2014. In 2017, he was a Finalist for the Best Paper Award in Electromagnetics and Antenna Theory at the 11th European Conference on Antennas and Propagation, Paris. In 2018, he was a co-recipient of the Best Paper Award in Electromagnetics and Antenna Theory at the 12th European Conference on Antennas and Propagation, London, U.K. In 2019, he was a recipient of the Young Scientist Award at the 41st Progress in Electromagnetics Research Symposium, Rome, Italy. In 2020, he got the National Scientific Habilitation for Associate Professorship of Electromagnetic Fields from the Italian Ministry of University and Research. In 2020, 2021 and 2022, he has been selected among the outstanding reviewers of the IEEE TRANSACTIONS ON ANTENNAS AND PROPAGATION. In 2021 to 2022, he has been recipient of the "Young Scientist Awards" at the XXXIV General Assembly and Scientific Symposium of the International Union of Radio Science (URSI-GASS 2021), and at 3rd URSI Atlantic Asia-Pacific Radio Science Meeting (URSI AT-AP RASC 2022), respectively. From 2023, he is a Chair of the AG "Young Professionals" of the IEEE Italy Section. Since 2022, he is also a URSI Senior Member. He serves as an Associate Editor for IEEE ACCESS, IET *Electronics Letters*, and *Frontiers in Antennas and Propagation*.



**MATTEO BRUNO LODI** (Member, IEEE) received the bachelor's degree in biomedical engineering from the University of Cagliari, Cagliari, in 2016, and the master's degree in biomedical engineering from Politecnico di Torino, Turin, Italy, in 2018. He is currently pursuing the Ph.D. degree in electronic engineering and computer science with the University of Cagliari. His research interests include the modeling of bioelectromagnetic phenomena, especially hyperthermia treatment; the study, manufacturing, and synthesis of magnetic biomaterials for tissue engineering applications; and the use of the microwave for biotechnology and environmental applications. He has been appointed as a Representative for the Young Professionals of IEEE Region 8 Nanotechnology Council. He is a member of the editorial board of *IEEE Future Directions Technology Policy and Ethics Newsletter*. He was awarded as the Young Scientist at the General Assembly and Scientific Symposium of URSI, in 2020 and 2021.



**NICOLA CURRELI** (Member, IEEE) received the M.Sc. degree from the University of Genoa, Genoa, Italy, in 2016, and the joint Ph.D. degree in electronic engineering from the University of Cagliari, Cagliari, Italy, and the Italian Institute of Technology (IIT), Genoa, in 2020. After completing the Ph.D. degree, he was a fellow with the Graphene Laboratories, IIT, within the Graphene Core 2 Project (Graphene Flagship). In 2019, he was a Visiting Researcher with the Department of Physics and the Mechanical Engineering Department, Columbia University, New York City, NY, USA, as a part of the Marie Skłodowska-Curie SONAR H2020 Action. Between 2022 and 2023, he was a Visiting Researcher with Molecular Foundry with the Lawrence Berkeley National Laboratory, Berkeley, CA, USA. He is currently a Postdoctoral Researcher with the Functional Nanosystems Group, IIT. His research interests include the study of low-dimensional materials, their characterization and their application in the field of photonics, and the design, implementation, and analysis of linear and nonlinear integrated optical, microwave devices, and antennas. He received the Young Scientists Award at the General Assembly and Scientific Symposium of URSI, in 2022. He is also a member of the Topical Advisory Panel of Photonics and an Academic Editor of the *Journal of Nanotechnology*. He is a part of the Committee of the Young Professionals Affinity Group, IEEE R8 Italy Section.



**GIACOMO MUNTONI** received the dual Graduate degree in electronic engineering and telecommunication engineering and the Ph.D. degree in electronic engineering and computer science from the University of Cagliari, in 2010, 2015, and 2019, respectively. He is currently a Technologist with the Applied Electromagnetics Group. His research interests include the design and characterization of antennas for biomedical and aerospace applications, microwave-based dielectric characterization of materials, 3-D printing of RF components, and the monitoring of the space debris environment in low earth orbit with the Sardinia radio telescope, in collaboration with the Cagliari Astronomical Observatory.



**ALESSANDRO FANTI** (Senior Member, IEEE) received the Laurea degree in electronic engineering and the Ph.D. degree in electronic engineering and computer science from the University of Cagliari, Cagliari, Italy, in 2006 and 2012, respectively. From 2013 to 2016, he was a Postdoctoral Fellow with the Electromagnetic Group, University of Cagliari, where he is currently an Assistant Professor. He has authored or coauthored 58 articles in international journals. His research interests include the use of numerical techniques for modes computation of guiding structures, optimization techniques, analysis and design of waveguide slot arrays, analysis and design of patch antennas, radio propagation in urban environment, the modeling of bioelectromagnetic phenomena, and microwave exposure systems for biotechnology and bioagriculture. He is a member of the IEEE Antennas and Propagation Society, Italian Society of Electromagnetism, National Interuniversity Consortium for Telecommunications, and Interuniversity Center for the Interaction Between Electromagnetic Fields and Biosystems. He is an Associate Editor of the *IEEE JOURNAL OF ELECTROMAGNETICS, RF AND MICROWAVES IN MEDICINE AND BIOLOGY*. Since 2020, he has been a Principal Investigator of the IAPC Project, funded with e5 million by the Italian Ministry of Economic Development (MISE), within the AGRIFOOD PON I&C (2014–2020) (CUP: B21B1900064008 COR: 1406652).



**GINO SORBELLO** (Member, IEEE) received the Laurea degree (cum laude) in electronics engineering from the University of Catania, Catania, Italy, in 1996, and the Ph.D. degree in electronics and communications engineering from the Polytechnic Institute of Milan, Milan, Italy, in 2000. He became an Assistant Professor in electromagnetic fields with the University of Catania, in 2002, where he has been an Associate Professor in electromagnetic fields with the Department of Electrical, Electronics, and Computer Engineering, since 2014. Since 2012, he has been a member of INFN-LNS and collaborates with the Ion Sources and Plasma Physics Group. His current research interests include single-mode solid-state waveguide lasers and amplifiers, integrated optics, the development of planar antennas and ultra-wideband compact antennas, the study of microwave devices and computational electromagnetism, RF-plasma interactions, and particle accelerators.



**GIUSEPPE MAZZARELLA** (Senior Member, IEEE) received the Graduate degree (summa cum laude) in electronic engineering from the University of Naples Federico II, in 1984, and the Ph.D. degree in electronic engineering and computer science, in 1989. In 1990, he became an Assistant Professor with Dipartimento di Ingegneria Elettronica, University of Naples Federico. Since 1992, he has been with Dipartimento di Ingegneria Elettrica ed Elettronica, Università di Cagliari, an Associate Professor and then, since 2000, as a Full Professor, teaching courses in electromagnetics, microwave, antennas, and remote sensing. He is the author or coauthor of over 70 articles in international journals. His research interests include the efficient design of large arrays of slots and the power synthesis of array factor, with an emphasis on the inclusion of constraints, microwave holography techniques for the diagnosis of large reflector antennas, and the use of evolutionary programming for the solution of inverse problems, in particular problems of synthesis of antennas and periodic structures. He is a reviewer of many EM journals.

...